Cubic Parametrization of the Deceleration Parameter Within f(T) Gravity Postprint

Authors: D. D. Pawar, N. G. Ghungarwar and P. S. Gaikwad

Date: 2025-06-13T16:50:50+00:00

Abstract

In this study, we used the f(T) gravity framework with the energy-momentum tensor for a perfect fluid to derive key cosmological parameters, including the Hubble parameter H, deceleration parameter q and Statefinder diagnostics. Model parameters were optimized using an R2 test, resulting in , , and , with an R2 of 0.9527. Our model aligns closely with the ΛCDM model and shows good performance based on AIC and BIC criteria. Analyzing the q(z) curve revealed the transition from deceleration to acceleration in the universe's expansion. Additionally,we examined pressure,energy density,and equation of state parameter for two models, f(T) = λT and f(T) = T + βT2,both aligning well with observational data. The r–s and r–q diagnostics further confirm our model's consistency with ΛCDM,making it a strong alternative for explaining cosmic expansion. The evolution of Ω(z) shows strong consistency with the ΛCDM model,with the Om parameter approaching 0.3 at lower redshifts and parameter uncertainties highlighting the model's reliability.

Full Text

Preamble

Research in Astronomy and Astrophysics, 25:065019 (19pp), 2025 June

https://doi.org/10.1088/1674-4527/add244
CSTR: 32081.14.RAA.add244

Cubic Parametrization of the Deceleration Parameter Within f(T) Gravity

D. D. Pawar[1], N. G. Ghungarwar[2], and P. S. Gaikwad[1]
[1] School of Mathematical Sciences, SRTM University, Nanded-431606, Maha-

rashtra, India; dypawar@yahoo.com, gaikwadpramod.pg@gmail.com
[2] Shri Dnyaneshwar Maskuji Burungale Science and Arts College, Shegaon-444203, Maharashtra, India; nghungarwar31@gmail.com

Received 2024 November 26; revised 2025 March 16; accepted 2025 April 21; published 2025 June 4

Abstract

In this study, we used the f(T) gravity framework with the energy-momentum tensor for a perfect fluid to derive key cosmological parameters, including the Hubble parameter H, deceleration parameter q, and Statefinder diagnostics. Model parameters were optimized using an R^2 test, resulting in values of 0.013, = 0.50, with an R^2 of 0.9527. Our model aligns closely with the ΛCDM model and shows good performance based on AIC and BIC criteria. Analyzing the q(z) curve revealed the transition from deceleration to acceleration in the universe's expansion. Additionally, we examined pressure, energy density, and equation of state parameter for two models, $f(T) = \lambda T$ and $f(T) = T + \beta T^2$, both aligning well with observational data. The r–s and r–q diagnostics further confirm our model's consistency with ΛCDM, making it a strong alternative for explaining cosmic expansion. The evolution of Ω(z) shows strong consistency with the ΛCDM model, with the Om parameter approaching 0.3 at lower redshifts and parameter uncertainties highlighting the model's reliability.

Key words: equation of state—gravitation—(cosmology:) dark energy—(cosmology:) large-scale structure of universe

1. Introduction

In recent years, modified gravity theories have gained significant attention as alternatives or extensions to general relativity (GR). One such theory is f(T) gravity, which is based on the idea of modifying the teleparallel equivalent of GR (TEGR) by introducing a function of the torsion scalar T. Unlike GR, which focuses on curvature, f(T) gravity takes torsion into account, providing a new perspective on gravitational interactions and the evolution of the universe.

The perfect fluid model is widely used in cosmology to describe the large-scale behavior of matter and energy in the universe. In the context of the Friedmann–Lemaître–Robertson–Walker (FLRW) cosmological model, which describes a homogeneous and isotropic universe, the perfect fluid offers a simple yet effective approach to model the distribution of matter, energy, and pressure. This model is essential for understanding the dynamics of the universe, including the expansion and the role of dark energy and dark matter.

Mohanty & Mishra (2001, 2003) made notable contributions to cosmological model studies, especially within Bianchi type cosmologies involving perfect fluid distributions. Their initial work focused on developing LRS Bianchi Type-I cosmological models in a perfect fluid framework, establishing a foundational

model. Building on this, they later introduced scale-invariant theories for Bianchi type VIII and IX spacetimes, broadening the approach to explore cosmological behaviors in more complex, anisotropic settings. Ferraro & Fiorini (2007) made a notable impact on modified gravity theories by introducing a model of modified teleparallel gravity. Their work presented a fresh perspective on cosmic inflation, showing it could occur without the need for an inflation field. This approach opened up new possibilities for explaining early universe dynamics within the teleparallel gravity framework. Building on this foundation, Bengochea & Ferraro (2009) explored the concept of dark torsion as a potential driver of the universe's accelerated expansion. Their study provided valuable insights, suggesting that teleparallel gravity could offer a compelling alternative to traditional explanations of cosmic acceleration.

Pradhan & Mathur (2009) and Pradhan & Ram (2009) investigated the dynamics of inhomogeneous cosmological models within Lyra geometry, focusing on perfect fluid universes influenced by electromagnetic fields and magnetic permeability variations. Their studies included a model of a perfect fluid universe with an electromagnetic field and a plane-symmetric, magnetized inhomogeneous cosmological model with variable magnetic permeability. These works provided valuable insights into how Lyra geometry can be applied to study inhomogeneous structures, expanding the understanding of the role of magnetic fields in the evolution of large-scale cosmic structures. Linder (2010) proposed an alternative approach to cosmic acceleration by examining a modified gravity theory, often referred to as "Einstein's other gravity." His work demonstrated how this modified gravity could account for the observed acceleration of the universe, offering a potential substitute for dark energy in cosmological models.

Chen et al. (2011) focused on cosmological perturbations within the framework of f(T) gravity. Their study shed light on how modifications in teleparallel gravity impact the behavior of cosmological perturbations, contributing to the development of alternative models of the early universe. Harko et al. (2011) introduced the f(R, T) gravity theory, where the gravitational Lagrangian is a function of both the Ricci scalar R and the trace of the energy-momentum tensor T. This theory opened new avenues for exploring modified gravity and its potential to explain cosmic phenomena without invoking dark matter or dark energy. Tamanini & Boehmer (2012) analyzed the tetrad choices in f(T) gravity, distinguishing between "good" and "bad" tetrads. Their work clarified how certain tetrad configurations impact the viability of solutions within teleparallel gravity, helping refine the use of f(T) gravity in cosmological models.

Duran et al. (2012) examined the matter power spectrum within dark energy models, using the Harrison-Zel'dovich prescription as a foundation. Their work offered insights into the compatibility of dark energy models with observed cosmic structures, contributing to a better understanding of matter distribution in the universe. Geng et al. (2012) investigated observational constraints on teleparallel dark energy models, focusing on how teleparallel gravity could explain dark energy phenomena. Their study provided valuable data on the vi-

ability of teleparallel gravity as an alternative framework for explaining cosmic acceleration. Setare & Darabi (2012) explored power-law solutions within f(T) gravity, presenting solutions that contribute to understanding the evolution of the universe under modified teleparallel gravity. Their work enriched the theoretical foundation of f(T) gravity models. Karami & Abdolmaleki (2012) studied the generalized second law of thermodynamics within f(T) gravity frameworks. Their research addressed thermodynamic properties in modified gravity models, offering insights into the thermodynamic viability of f(T) gravity.

Singh & Singh (2014) and Rao et al. (2014) developed perfect fluid cosmological models within a modified theory of gravity, examining how these models influence cosmic dynamics. Their work contributed to exploring alternative cosmological models that incorporate perfect fluid distributions in non-standard gravitational frameworks. Harko et al. (2014) extended f(T) gravity by introducing nonminimal torsion-matter coupling, providing a novel perspective on interactions between torsion and matter. This work helped deepen understanding of modified teleparallel gravity and its potential applications in cosmology. Junior et al. (2015) studied Born-Infeld and charged black holes within f(T) gravity, considering the effects of nonlinear sources. Their research expanded the theoretical landscape of black hole solutions in modified gravity frameworks. Rani et al. (2015) developed Bianchi type-III magnetized string cosmological models within f(R, T) gravity, incorporating perfect fluid distributions. Their work contributed to understanding how magnetized cosmologies evolve under modified gravitational theories. Mishra et al. (2015) proposed a dark energy cosmological model for Bianchi type-III spacetime with a perfect fluid. This study provided insights into how dark energy can be modeled within anisotropic spacetimes. Shaikh (2016) examined a binary mixture of perfect fluid and dark energy in modified gravity, offering an alternative framework for understanding dark energy and perfect fluid interactions within cosmological models.

Nunes et al. (2016) investigated the cosmological viability of non-Gaussian statistics in dark energy models, contributing to understanding statistical features in cosmological observations under alternative gravity frameworks. Cai et al. (2016) explored f(T) teleparallel gravity in cosmology, presenting a comprehensive overview of how this theory can address various cosmological phenomena, including dark energy and inflation. Krššák et al. (2019) reviewed teleparallel theories of gravity with a focus on achieving a fully invariant approach. Their work illuminated the foundational aspects of teleparallel gravity, enhancing its utility in theoretical physics and cosmology. Arora et al. (2020) focused on observational constraints for f(Q, T) gravity models, offering a detailed analysis of how these models align with observed cosmic phenomena. Their work strengthened the case for f(Q, T) gravity as a viable alternative in the study of cosmological evolution. Sahoo et al. (2020) developed a mixed fluid cosmological model within f(R, T) gravity, focusing on interactions between different fluid types in the context of modified gravity. This model provided insights into the dynamics of cosmic evolution within f(R, T) gravity frameworks. Pradhan et al. (2020) examined transit cosmological models under f(Q, T) gravity, placing

particular emphasis on observational constraints. Their work contributed to understanding how f(Q, T) gravity can align with observed cosmic phenomena, especially in models where transit behavior is key.

Tiwari et al. (2020) studied phase transitions in LRS Bianchi type-I cosmological models within f(R, T) gravity, focusing on how phase transitions affect cosmological evolution. Their work offered a new perspective on the role of modified gravity in cosmic phase transitions. Pawar et al. (2021) investigated perfect fluid and heat flow within the f(R, T) gravity framework. Their study provided an analytical approach to understand heat flow dynamics in modified gravity theories, particularly within perfect fluid cosmologies. Mandal & Sahoo (2021) explored constraints on the equation of state (EoS) parameter (ω) in non-minimally coupled f(Q) gravity. Their work examined how varying ω affects the behavior of the universe under this modified gravity framework, offering insights into the parameter's cosmological implications. Pawar & Mapari (2022) developed a plane-symmetry cosmological model with an interacting field in f(R, T) gravity, examining how interactions influence cosmological evolution. Their model added depth to the study of interacting fields in modified gravity frameworks. Duchaniya et al. (2022) conducted a dynamical stability analysis of accelerating f(T) gravity models, focusing on the conditions that ensure stable cosmic acceleration. Their findings advanced the understanding of stability in teleparallel gravity models. Kumar et al. (2023) investigated the phase structure and critical behavior of charged-AdS black holes in the presence of perfect fluid dark matter. Their study provided valuable insights into the thermodynamic properties of black holes in modified gravity and dark matter contexts. Naicker et al. (2023) analyzed isotropic perfect fluids within modified gravity, focusing on how isotropy affects the viability of perfect fluid models under alternative gravitational theories. Their work contributed to understanding fluid dynamics in modified gravity contexts. Solanke et al. (2023) examined anisotropic dark energy models within f(Q, T) gravity, using observational constraints to assess model viability. Their work added to the study of dark energy in modified gravity, especially for anisotropic cosmological models. Tiwari et al. (2023) proposed a transition model in f(R, T) theory, using observational constraints to examine transition behaviors in modified gravity. This model contributed to understanding how transitions influence cosmic evolution within f(R, T) gravity. Singh et al. (2023) developed a constrained cosmological model within Lyra geometry, examining how Lyra geometry affects cosmic dynamics under modified constraints. Their work expanded the applications of Lyra geometry in cosmological models. Pradhan et al. (2023) proposed an f(R, T)-based FLRW model with observational constraints, investigating how f(R, T) gravity can support FLRW cosmology in observed conditions. This study added to the literature on FLRW models within modified gravity. Narawade & Mishra (2023) explored a phantom cosmological model in f(Q) gravity, considering observational constraints to assess the model's viability. Their work contributed to understanding phantom energy's role in cosmological expansion within modified gravity. Shekh et al. (2023) analyzed observational constraints in an accelerated emergent f(Q)

gravity model. Their work provided valuable insights into how observational data can support accelerated cosmic expansion within the f(Q) gravity framework. Pawar et al. investigated the anisotropic behavior of perfect fluid within fractal cosmology, offering new perspectives on how fractal geometry influences anisotropic cosmic structures. Their study contributed to the broader understanding of anisotropy in cosmological models.

In recent years, modified gravity theories have gained significant attention as viable alternatives to GR, particularly in explaining cosmic acceleration and astrophysical phenomena. Pawar et al. (2025b) investigated the implications of f(R, T) gravity on quark and strange quark matter, providing observational constraints that highlight modified gravity's influence in high-density astrophysical environments. In a related study, Pawar et al. (2025a) explored the dynamics of a perfect fluid within the framework of f(T) gravity, demonstrating how observational constraints shape the cosmic evolution predicted by torsion-based modifications. Shukla et al. (2025) further examined the role of f(T) gravity in driving the late-time acceleration of the universe, emphasizing its ability to replicate cosmic expansion history without invoking a cosmological constant. Moreover, Chen et al. (2024) assessed the potential of next-generation gravitational-wave detectors in constraining f(T) gravity, paving the way for novel observational tests of teleparallel modifications. Additionally, Malik et al. (2024) investigated physically viable solutions for anisotropic hybrid stars within f(T) gravity using an embedding approach, demonstrating that such models can effectively describe compact stellar structures. These recent developments underscore the growing significance of f(T) gravity in addressing key challenges in both cosmology and astrophysics, motivating further exploration of its theoretical and observational implications.

Sood et al. (2024) explored photon orbits and phase transitions in Letelier AdS black holes immersed in perfect fluid dark matter. This research enriched the study of black hole physics by examining how dark matter affects photon trajectories and phase behaviors in AdS black holes. Pawar et al. (2024c) developed a fractal cosmological model featuring two forms of dark energy, guided by a specific Hubble parameter. Their study offered insights into dark energy's role in fractal cosmology, highlighting the implications of multiple dark energy components on cosmic expansion. Pawar et al. (2024d) examined observational constraints on the wet dark fluid model within fractal gravity. Their research assessed how wet dark fluid behaves under fractal gravity, contributing to the study of alternative dark energy models. Yadav et al. (2024) focused on reconstructing f(Q) gravity from Hubble parameter parameterization and observational constraints, offering a framework to link f(Q) gravity with empirical data on cosmic expansion. Pawar et al. (2024b) studied perfect fluid with heat flow in the f(T) theory of gravity, examining how heat flow interacts with perfect fluids under teleparallel gravity. Their work added a thermal perspective to f(T) cosmology. Pawar et al. (2024a) developed a model involving two fluids in f(T) gravity, using observational constraints to assess its viability. This research contributed to understanding the role of multi-fluid systems in teleparallel gravity,

especially under observationally constrained conditions.

Our work stands out due to (i) a novel parameterization approach, (ii) a comparative analysis of two prototype f(T) models within this framework, (iii) extensive observational constraints using multiple diagnostic tools, and (iv) a strong connection to Lambda Cold Dark Matter (ΛCDM) and established diagnostics. We propose a cubic parameterization of the deceleration parameter q(t) in f(T) gravity, inspired by Sofuoğlu et al. (2023), but uniquely applied in a teleparallel setting. Unlike traditional f(T) studies that assume specific functional forms of f(T) or parameterize dark energy's EoS, our approach directly parameterizes q(t). This enables an analytical derivation of the Hubble parameter and scale factor, offering a model-agnostic perspective on cosmic expansion.

We examine two representative f(T) models: (I) $f(T) = \lambda T$ (teleparallel GR equivalent) and (II) $f(T) = T + \beta T^2$ (a quadratic extension). While both models have been individually studied, our comparative analysis under identical constraints highlights their response to the same expansion history. Our findings show that both models closely mimic ΛCDM, reinforcing the consensus that many viable f(T) models resemble standard cosmology at the background level.

Unlike purely theoretical studies, our work is data-driven. Using Hubble parameter measurements from the Observational Hubble Dataset (OHD), we apply model selection criteria (Akaike Information Criterion (AIC), Bayesian Information Criterion (BIC)) and introduce an R^2 goodness-of-fit metric alongside ^{2}. Furthermore, we perform statefinder diagnostics (r, s and r, q) and the Om diagnostic, explicitly comparing our model's behavior with established dark energy models. The close alignment with ΛCDM strengthens the validity of our approach. To position our study within the latest developments in f(T) cosmology, we incorporate recent works, such as Wang & Mota (2020) on H_0 tension. Our best-fit $H_0 = 72.6 \pm 0.5$ km s^{-1} Mpc^{-1} aligns well with recent direct measurements, contributing to the ongoing H_0 tension discussion. A key novelty of our study is the explicit analysis of q(z) evolution. While many f(T) studies focus on H(z), we emphasize the transition redshift (q = 0). Our best-fit model predicts z_{trans} 0.6, consistent with observational estimates (z 0.5–0.7). This detailed investigation of q(z) further differentiates our work within the field.

The main goal of this study is to explore how the pressure, density, and EoS parameters behave within the framework of f(T) gravity. These parameters are key to understanding the relationship between matter, energy, and the expansion of the universe. In addition to the EoS, this research will also investigate other important diagnostics, such as statefinder parameters and stability conditions, to assess the viability and observational consequences of f(T) gravity. By analyzing these parameters, we aim to gain deeper insights into the influence of f(T) gravity on the evolution of the cosmos and how it compares with more conventional models like GR. This paper is organized as follows: Section 1—Introduction, Section 2—Field Equations, Section 3—Cosmological Parameters, and Section 4—Discussion and Conclusion.

2. Field Equations

We investigate the FLRW metric studied by Izumi & Ong (2013), which is expressed as $ds^2 = dt^2$ - $a(t)^2dx^2$. The scale factor a(t), which varies with cosmic time t, governs the universe's expansion or contraction. The components of the tetrad are defined by e^a_ = diag(1, a(t), a(t), a(t)). In this framework, f(T) is a differentiable function of T, where T denotes the torsion scalar from teleparallel gravity. The term L_{matter} denotes the matter Lagrangian density, while e is the determinant of the tetrad field. This determinant is related to the metric tensor by the relation g = _{ab}e^a– ^{e}b_ .

The torsion scalar T studied by Capozziello et al. (2013) is given by T = -$6H^2$, where H = ȧ/a is the Hubble parameter. In this equation, the torsion tensor S with indices , , and represents the asymmetry in the connection, capturing the deviation from a symmetric connection in the theory. It describes the geometric effects of torsion. The components of the torsion tensor S^ _{ } are defined as S^ _{ } = ½(K^ _{ } + δ– ^{T}α{α } - δ– ^{T}α{α }), where K^ _{ } is the contorsion tensor. The antisymmetric tensor, denoted by T_{ }, emphasizes the non-symmetric aspects of the torsion tensor. It highlights the asymmetric nature of the connection in a mathematical sense. The components of this tensor satisfy the condition T_{ } = -T_{ }, capturing the antisymmetric properties of the torsion tensor.

The contorsion tensor is defined by the equation K^ _{ } = -½(T^ _{ } - T_ ^ _ + T_ ^ _). The modified field equation in teleparallel gravity is obtained by varying the action with respect to the vierbein components h_i^ and is given by:

e^{-1} *(eS_a^{ })f_T* - $e^{-\{aT\}}$ { σ}S_ ^{σ }f_T + ¼e^ _{af}(T) = ¼eT^ _a

where f_T = df/dT, and T^ _a is the energy-momentum tensor.

Our model uses the standard minimal coupling between matter and gravity (the matter Lagrangian L_{matter} enters additively in the action). The phrase "nonlinear Lagrangian matter coupling" in our context refers to the fact that the gravitational Lagrangian contains a nonlinear function of the torsion scalar, f(T). This modifies how the matter content influences cosmic dynamics. In GR (or its teleparallel equivalent, TEGR), which corresponds to f(T) = T, the field equations (Friedmann equations) relate the Hubble expansion directly to the energy density and pressure p of matter.

The energy-momentum tensor for a perfect fluid investigated by Dimakis et al. (2014) is given by T_{ } = (+ p)u_ u_ - pg_{ }, where p denotes the pressure and represents the energy density of the fluid. The four-velocity vector in the comoving coordinate system is u^ = (0, 0, 0, 1), which satisfies the conditions u^ u_ = 1 and u^ _ u_ = 0.

The trace provides valuable information about the total energy distribution and pressure within a system, helping us understand the gravitational effects on

spacetime. The trace is calculated as T = g^{ }T_{ } = - 3p.

The torsion scalar T is a geometric quantity used in modified gravity theories to measure the deviation of a torsion-based connection from a torsion-free one. In teleparallel gravity, T is derived from the torsion tensor components. Its specific form depends on the chosen gravitational theory and plays a crucial role in describing spacetime geometry. We compute the torsion scalar T as follows: T = -6H^2.

The field equation from the variation of the action, when applied to the FLRW metric, simplifies to:

3H^{2}f_T + ½(f - Tf_T) =

2Hf_T + 3H^{2}f_T + ½(f - Tf_T) = -p

Here, a dot above a field variable denotes differentiation with respect to time t.

We adopt the deceleration parameter as proposed by Sofuoğlu et al. (2023):

q(t) = -1 + (n$_1$t)/(1 + n$_2$t^2)

where n$_1$ and n$_2$ are positive constants. Given the relation between the Hubble parameter and the deceleration parameter, q(t) = -äa/ȧ^2, and using this along with the definition of q(t), we obtain:

H(t) = (n$_1$t)/(1 + n$_2$t^2)

To determine the scale factor, we use the relation H(t) = ȧ/a along with the expression for H(t), yielding:

a(t) = β(1 + n$_2$t^2)^{n$_1$/(2n$_2$)}

where β is a positive constant of integration and = n$_1$/(2n$_2$). Substituting this into the metric, we obtain the complete spacetime description.

From Figure 1, we observe that the scale factor a(t) begins near zero, indicating a very compact universe (consistent with a Big Bang origin). As t increases, a(t) grows gradually at first (decelerating expansion), and then much more rapidly at later times. We highlight the "sharp upward trend" of a(t) at late times, which signifies the transition to accelerated expansion. This qualitative behavior—slow expansion in the past followed by recent acceleration—aligns with the established ΛCDM narrative and observations of cosmic history.

3. Cosmological Parameters

In this section, we explore key cosmological parameters, including the Hubble parameter, model comparison using AIC and BIC, the deceleration parameter, the EoS parameters for both Model I and Model II, and the statefinder diagnostic. Each of these parameters is examined in detail below.

3.1. Hubble's Parameter

The Hubble parameter H(t) is a fundamental concept in cosmology that measures the rate of the universe's expansion at any given time t. By tracking how H(t) changes over time, we can observe the universe's evolving expansion rate, influenced by factors such as dark energy, matter, and radiation. This time-dependent parameter helps reveal different expansion phases, such as periods of acceleration and deceleration, offering valuable insights into the universe's overall history.

In this study, we express the Hubble parameter in terms of both cosmic time t and redshift z. The expression for the Hubble parameter as a function of cosmic time is:

$H(t) = (n_1 t)/(1 + n_2 t^2)$

where $n_1 > 0$ and $n_2 > 0$ are constants.

The Hubble parameter as a function of redshift is expressed as:

H(z) = H_0(1 + z)^{1+ }

This form shows how the Hubble parameter changes with redshift, providing insights into how the expansion rate evolves with observable distance. By incorporating redshift z, we connect the present expansion rate to the universe's past, allowing us to capture a comprehensive picture of cosmic evolution.

Figure 2 presents the relationship between the Hubble parameter H(z) and redshift z. The vertical axis signifies H(z) in km s^{-1} Mpc^{-1}, spanning from 0 to 250, while the horizontal axis represents z, covering a range from 0 to 2.5. Observational data points obtained via the Differential Age (DA) method are depicted as purple circles, whereas Baryon Acoustic Oscillations (BAO) data are shown as yellow diamonds, both with error bars indicating measurement uncertainties. The red solid line represents the best-fit f(T) model prediction, while the blue dashed line corresponds to the ΛCDM prediction based on Planck reference parameters ($H_0 = 67.8$, Ω_{m0} = 0.3, Ω_Λ0 = 0.7).

This figure is pivotal in demonstrating our model's alignment with observational H(z) data. Our discussion emphasizes that the model's curve closely follows the ΛCDM trajectory across the entire redshift range, passing through the central regions of the data point error bars, indicating an excellent fit. Minor deviations at higher redshifts ($z > 1.5$) are analyzed, showing slight differences that further confirm the ability of f(T) gravity to emulate ΛCDM behavior effectively. Moreover, the minimal scatter of data points around our model curve visually supports the high R^2 value, reinforcing the robustness of the fit. This figure provides a crucial foundation for understanding the optimized parameters detailed in Table 1.

We determined the best-fit curve for H(z) using 57 observed data points and the R^2-test. The R^2-test refers to the coefficient of determination R^2, a statistical

measure that indicates how well data points fit a model or regression line. The R^2 value ranges from 0 to 1, with $R^2 = 1$ indicating a perfect fit (the model explains 100% of the variance in the data) and lower values indicating a less perfect fit. By contrast, the ^{2} test (chi-square) is a goodness-of-fit measure that sums the squared differences between observations and model predictions weighted by the observational uncertainties.

The R^2-test evaluates how well the independent variable explains the variation in the dependent variable. An R^2 value of 1 implies a perfect fit between our model parameters H_0 and and the OHD. For this analysis, we focused on data within the redshift range z > -1 to determine the best-fit values for H_0 and . Error bars indicate the mean and standard deviation for the 57 Hubble data points, and we compared our model to the well-known ΛCDM model, with H_0 = 67.8 km s^{-1} Mpc^{-1}, Ω_Λ0 = 0.7, and Ω_{m0} = 0.3 representing the density parameters for dark energy and matter. This comparison is illustrated in Figure 3. The best-fit values we obtained are $\beta = 1.312$, = 1.273, and H_0 = 72.60 km s^{-1} Mpc^{-1}, with an R^2 of 0.9527 and an RMSE of 9.2501.

The table summarizes key results from the cosmological model fitting. The parameter β is estimated to be 1.312, and is 1.273, both with small uncertainties, suggesting reliable measurements. The Hubble constant H_0, representing the universe's current expansion rate, is found to be 72.60 km s^{-1} Mpc^{-1}, consistent with the findings of Kolhatkar et al. (2024). With an R^2 value of 0.9527 and an RMSE of 9.2501, the model demonstrates a strong fit to the data. The covariance matrix provides insight into parameter uncertainties and their correlations; small off-diagonal values here imply minimal correlation between β, , and H_0, indicating that the data constrain each parameter robustly and largely independently. This helps to understand why the error bars on β and are so small—the fit is very tight and the parameters are well determined. Thus, the covariance matrix is an important by-product of our curve-fitting procedure, confirming the reliability of the parameter estimates and allowing us to propagate uncertainties to other derived quantities.

In Figure 3, the shaded regions around the best-fit curve represent the 1σ (68% confidence) and 2σ (95% confidence) uncertainty bands for the model's Hubble parameter H(z) as a function of redshift. These bands are derived from the covariance matrix of the parameters. In practice, we propagated the parameter uncertainties (assuming a Gaussian error distribution for the parameters β and and their covariance) to compute the uncertainty in H(z) at each redshift. The result is a predicted range of H(z) values at each z corresponding to the 68% confidence region (dark shaded area) and the 95% region (lighter shaded area). Thus, the shaded regions in Figure 3 visually convey how certain we are about our model prediction given the data uncertainties—they show the confidence intervals around the best-fit H(z) curve.

3.2. Model Comparison

To evaluate the reliability of our model, we used two statistical tools: the AIC and the BIC. These criteria help us determine how well our model fits the data while accounting for model complexity.

The AIC is calculated as follows:

AIC = ^{2}_{min} + 2d

where d is the number of parameters in the model. To compare our model with the standard ΛCDM model, we define the difference in AIC as ΔAIC = AIC_{Model} - AIC_ΛCDM. An AIC difference between 4 and 7 suggests moderate support for our model, while a difference less than 2 indicates strong support. If the ΔAIC exceeds 10, it suggests weak support for our model.

The BIC is calculated as:

BIC = ^{2}_{min} + d ln(N)

where N is the number of data points in our analysis. Similar to AIC, we define ΔBIC to compare models. A ΔBIC between 2 and 6 suggests moderate support, while a value less than 2 indicates strong support.

To evaluate the fit of our model to the data, we calculate the difference, or residual, between each observed value of H_{obs}(z) and the corresponding model prediction H(z). We then square these residuals, weigh them by the uncertainties in each observation, and sum them all together. This sum gives us the chi-squared value, ^{2}, which is defined as:

^{2} = Σ_i [H_{obs}(z_i) - H(z_i; H_0, β,)]^2/σ_i^2

For our model, we obtained AIC_{Model} = 37.49 and BIC_{Model} = 43.82, calculated using a minimum chi-squared value of ^{2}_{min} = 31.49, which results in ΔAIC = 2.51 and ΔBIC = 1.18. In comparison, the ΛCDM model has values of AIC_ΛCDM = 40 and BIC_ΛCDM = 45. These results, consistent with the findings of Jaybhaye et al. (2024), suggest that our model is moderately supported according to the AIC and strongly supported according to the BIC. This indicates that our model provides a competitive fit to the data compared to the standard ΛCDM model. By balancing both accuracy and simplicity, our model stands as a promising alternative in cosmological modeling.

3.3. Deceleration Parameter

The deceleration parameter q(t) provides insight into the rate at which the universe's expansion is slowing down or accelerating over cosmic time. By relating the scale factor to redshift, we can express q(t) as a function of time t. Initially, we define q(t) in terms of cosmic time as:

$q(t) = -1 + (n_1 t)/(1 + n_2 t^2)$

At early times (high redshift), q(z) approaches a positive value, characteristic of a matter-dominated era. In contrast, at low redshift, as z → -1, q(z) trends toward a negative value, approaching -1 if the expansion becomes de Sitter-like.

To understand q(z) in terms of redshift z, we derive its expression as a function of redshift. The redshift-dependent deceleration parameter is given by:

q(z) = -1 + (1 + z)^{- }

This form of q(z) provides a framework for understanding the expansion history of the universe and how it transitions from decelerating to accelerating phases over time.

Figure 4 shows how the deceleration parameter q(z) changes with redshift z, providing insights into the evolution of cosmic expansion. A key feature in the graph is the transition phase, marked by the point where q(z) crosses zero (indicated by the red dashed line). This transition highlights the shift from a decelerating universe to an accelerating one as the universe evolves over time. The central values of q(z) are shown by the main curve, while the shaded regions represent uncertainties in the parameters β and , illustrating the range of possible values based on model uncertainties. Spanning a redshift range from approximately -1.0 to 3.5, the figure captures both the past and potential future expansion phases, demonstrating how the universe has moved from a period of deceleration to its current phase of accelerated expansion. We also describe the asymptotic behavior of the deceleration parameter: at high redshift, q(z) approaches 0.5, consistent with matter domination, while at z → -1, q(z) → -1, indicating a de Sitter-like future.

3.4. Equation of State Parameter

In this section, we explore the relationship between energy density, pressure, and the EoS parameter as functions of cosmic time t and redshift z, by applying two different models: Model-I with f(T) = λT and Model-II with f(T) = T + βT^2.

The expression for the energy density is derived by solving the relevant field equation:

= (3H^2f_T - ½(f - Tf_T))

The pressure p is obtained by substituting into the field equations:

p = -(2Hf_T + 3H^2f_T - ½(f - Tf_T))

The EoS parameter ω is defined as the ratio of pressure to energy density, ω = p/ . Using the expressions for p and , we can write ω as:

ω = [-(2Hf_T + 3H^2f_T - ½(f - Tf_T))]/[3H^2f_T - ½(f - Tf_T)]

This formulation provides insight into the dynamics of cosmic acceleration and deceleration within the framework of the two models.

3.4.1. Model-I: f(T) = λT For Model-I, we consider f(T) = λT, where λ is a constant. In this setup, f_T = λ and f_{TT} = 0, making it a linear extension of TEGR. This linear form is notable because it preserves the second-order nature of the field equations, simplifying the analysis while still allowing for deviations that can explain cosmological effects, such as the universe's accelerated expansion. Model-I is particularly useful for examining straightforward modifications to GR that remain mathematically tractable.

The expression for energy density as a function of cosmic time t is:

(t) = 3λH^2

The energy density in terms of redshift z is:

(z) = 3λH$_0{}^2$(1 + z)^{2(1+)}

Figure 5 presents the evolution of the energy density (z) as a function of redshift, providing insights into the changing matter content of the universe over cosmic time. The blue curve represents the best-fit model based on the optimized parameter values β = 1.312 and = 1.273. As expected, energy density increases with redshift, reflecting the higher density of the early universe where matter played a dominant role in cosmic dynamics. The green and red shaded regions indicate the uncertainty ranges associated with variations in β and , respectively. The significant overlap of these bands suggests that while both parameters contribute to the model's uncertainty, the general trend remains stable and well-constrained. At z = 0, (0) aligns with the current matter density of the universe, approximately 0.1 in critical density units, consistent with observational estimates. Overall, this plot highlights the robustness of the model's predictions. Despite small parameter variations, the fundamental matter density evolution remains consistent, reinforcing the model's reliability in describing cosmic expansion.

The pressure in terms of cosmic time t is:

p(t) = -λ(2H + 3H^2)

The pressure in terms of redshift z is:

p(z) = -λH$_0{}^2$[2 (1 + z)^{2+ } + 3(1 + z)^{2(1+)}]

Figure 6 illustrates the evolution of pressure p(z) as a function of redshift z, with the best-fit curve (blue line) derived from the parameters β = 1.312 and = 1.273. This curve shows a decreasing trend in p(z) as redshift increases, suggesting that pressure was significantly higher in the early universe and gradually declined over cosmic time. The shaded regions represent the uncertainties associated with the parameters: the green band indicates the range due to the uncertainty in β, while the red band shows the effect of uncertainty in . The overlap between these bands suggests that the model is relatively stable despite variations in these parameters. Overall, this plot highlights a steady decline in cosmic pressure, with only minor sensitivity to changes in β and , reinforcing the robustness of the model in describing the universe's expansion history.

Figure 6 further illustrates the pressure evolution in Model I, showing that p(z) starts near zero at z = 0—consistent with pressureless dust at late times—and gradually becomes more negative as redshift increases. This behavior reflects the growing influence of the torsion term, which, in Model I ($\lambda \neq 0$), behaves like an effective cosmological constant and drives cosmic acceleration. As the universe evolved, p(z) declined, reaching strongly negative values in the present era. The uncertainty bands widen at higher redshifts, indicating that constraints on pressure are less precise at early times—an expected outcome since our model is primarily constrained using H(z) data up to z 2. The fact that p(z) becomes increasingly negative at lower redshifts strongly supports the idea that cosmic acceleration is driven by an effective dark energy component or modified gravity effects. This behavior aligns well with standard cosmological expectations, reinforcing the validity of our model in capturing the late-time acceleration of the universe.

The EoS parameter ω, which describes the relationship between pressure and energy density in cosmology, can be expressed in terms of cosmic time t as:

ω(t) = -1 - (2H)/(3H^2)

Alternatively, in terms of redshift z, the EoS parameter is given by:

ω(z) = -1 + 2 /(3(1 +))^{- }

These forms of ω allow us to understand how the EoS evolves over time or with redshift, providing insights into the dynamic behavior of the universe's expansion.

Figure 7 illustrates the evolution of the EoS parameter ω(z) with redshift z. The blue line represents the best-fit model, calculated with $\beta = 1.312$ and = 1.273. At high redshift, ω(z) is close to 0, indicating a matter-dominated era (since for dust $\omega = 0$). As z decreases, ω(z) drops and approaches -1 at z = 0 and into the future, indicating the emergence of a cosmological-constant-like behavior (de Sitter fate). We highlight that around the current epoch, ω in our model is around -0.9, which is slightly above -1 and consistent with a slowly varying dark energy component. This is expected since our model mimics ΛCDM (which has ω = -1 exactly for the cosmological constant). The slight deviation from -1 is due to the specific functional form of f(T) and the fact that Model I is effectively ΛCDM with a twist. We also mention in the text that the transition of ω(z) from 0 to near -1 is another way to see the deceleration-to-acceleration transition. The uncertainty bands (green for β, red for) show the sensitivity of ω(z) to parameter uncertainties. Overall, we explain that Figure 7 confirms that Model I behaves like a dark-energy-matter mixed universe, with an effective EoS shifting from 0 to -1 today, consistent with observations.

3.4.2. Model-II: f(T) = T + βT^2 For Model-II, we assume f(T) = T + βT^2, which gives f_T = 1 + 2βT and f_{TT} = 2β. This quadratic model introduces a nonlinear term in the torsion scalar T, allowing for a wider range of

cosmological solutions. By including the βT^2 term, the model can address both early universe inflation and late-time cosmic acceleration, potentially without invoking dark energy. Despite the added complexity, the field equations remain second-order, making this model both flexible and consistent with observational data.

The energy density in terms of cosmic time t is:

$(t) = 3H^2 + 18\beta H^4$

The energy density in terms of redshift z is:

$(z) = 3{H_0}^2(1 + z)\hat{}\{2(1+)\} + 18\beta {H_0}^4(1 + z)\hat{}\{4(1+)\}$

Figure 8 shows how energy density (z) changes with redshift z, using best-fit values for the model parameters: $\beta = 1.312$ and $= 1.273$. The blue line depicts the central prediction, revealing a sharp increase in (z) as redshift rises, which aligns with the idea that the universe was denser in its early stages. The green and red shaded areas reflect the impact of uncertainties in β and , respectively. The evolution of (z) in Model II is nearly identical to that in Model I at late times. This similarity is expected because both models are fitted to the same H(z) data, leading to a nearly identical background evolution. The figure confirms that the energy density increases as a function of z, reflecting a higher matter density in the past. The overlap between Model I and Model II curves suggests that the additional T^2 term in Model II primarily influences higher derivatives or subtle differences that are not significantly apparent in the redshift range considered. Any deviations from Model I would be more noticeable at earlier cosmic times or in effective EoS behavior.

The pressure in terms of cosmic time t is:

$p(t) = -(2H + 3H^2) - 2\beta(12H^2H + 18H^4)$

The pressure in terms of redshift z is:

$p(z) = -{H_0}^2[2\ (1 + z)\hat{}\{2+ \} + 3(1 + z)\hat{}\{2(1+)\}] - 2\beta {H_0}^4[12\ (1 + z)\hat{}\{4+ \} + 18(1 + z)\hat{}\{4(1+)\}]$

Figure 9 illustrates the evolution of pressure p(z) with redshift z, with the best-fit curve (blue line) derived from the parameters $\beta = 1.312$ and $= 1.273$. The curve shows a decreasing trend in p(z) as redshift increases, suggesting that pressure was higher in the past. The widening of the uncertainty bands at higher redshifts shows the model's sensitivity to variations in β and .

The evolution of pressure p(z) in Model II is similar to Model I: p(z) decreases with redshift, with negative pressures at late times driving cosmic acceleration. The overall trend closely follows that of Model I, reinforcing the idea that both models predict a declining pressure profile. A potential quantitative difference arises at $z = 0$, where Model II might exhibit slightly more negative pressure due to the influence of the βT^2 term, which can act as a mild effective cosmological

constant. The uncertainty bands indicate that variations in β and do not significantly affect the qualitative trend of pressure evolution.

The EoS parameter in terms of cosmic time t is:

$\omega(t) = [- (2H + 3H^2) - 2\beta(12H^2H + 18H^4)]/[3H^2 + 18\beta H^4]$

The EoS parameter in terms of redshift z is:

$\omega(z) = [-H_0{}^2[2\ (1 + z)\hat{}\{2+\ \} + 3(1 + z)\hat{}\{2(1+\ )\}] - 2\beta H_0{}^4[12\ (1 + z)\hat{}\{4+\ \} + 18(1 + z)\hat{}\{4(1+\ )\}]]/[3H_0{}^2(1 + z)\hat{}\{2(1+\ )\} + 18\beta H_0{}^4(1 + z)\hat{}\{4(1+\ )\}]$

Figure 10 shows the evolution of the EoS parameter $\omega(z)$ with redshift z, based on best-fit values $\beta = 1.312$ and $= 1.273$. The blue line represents the best-fit prediction, while the green and red bands illustrate the uncertainty ranges for β and , respectively. The effect of 's uncertainty is more pronounced, particularly at lower redshifts.

The EoS parameter $\omega(z)$ for Model II is similar to Model I: $\omega(z)$ starts near 0 and approaches -1 at z = -1. However, a slight dynamic feature emerges due to the T^2 term, causing a subtle difference in $\omega(z)$ evolution. Notably, at very high redshifts, $\omega(z)$ appears to transition from negative back to positive, which suggests that in an early epoch not explicitly modeled here, ω could become positive (e.g., during a radiation-dominated era). We clarify that our model is valid within the redshift range covered by our data (z 2.5). A key result from this figure is that the impact of the βT^2 term remains mild—Model II's $\omega(z)$ is nearly indistinguishable from Model I's within the observed redshift range. This finding reinforces the idea that even with a T^2 modification, the expansion history remains remarkably close to ΛCDM-like behavior. This contributes to our broader conclusion that f(T) models constrained by current data tend to closely mimic standard cosmology.

3.5. Statefinder Diagnostic

The Statefinder diagnostic is a valuable tool in cosmology that helps characterize the expansion history of the universe and provides insights into the nature of dark energy. This diagnostic technique enables us to distinguish between different cosmological models by leveraging observational data.

In this analysis, we computed the Statefinder parameters r and s, which trace the evolution of dark energy across various stages. These parameters are expressed in terms of the scale factor and are given by:

$r = äa/(aH^3)$ $s = (r - 1)/[3(q - ½)]$

where H is the Hubble parameter and q is the deceleration parameter.

By using these formulas we get:

$r(z) = 1 + (9/2)\ (1 + z)\hat{}\{-\ \}$ $s(z) = \ (1 + z)\hat{}\{-\ \}/[\ (1 + z)\hat{}\{-\ \} - ½]$

Figure 11 shows the evolution of r(z) as a function of redshift z, reflecting changes in the universe's expansion over time. At high negative redshift values, r(z) begins above 40, indicating a distinct early universe phase. As z approaches zero and beyond, r(z) decreases and stabilizes near 1, aligning with the ΛCDM model represented by the dashed line at r(z) = 1. The orange and blue shaded regions illustrate the uncertainties in the parameters β and . For $\beta = 1.312$ and = 1.273, these bands show the range of possible values for r(z) given parameter variations, offering insights into model robustness and the expansion dynamics of the universe. The statefinder r(z) in our model starts at high values in the distant past; r is well above 1 for z < 0.5 in our model, indicating a deviation from the simple ΛCDM value of 1 at early times. As z decreases toward 0, r(z) declines and approaches 1, indicating that the cosmic jerk is consistent with that of the ΛCDM model.

We have calculated s(z) as:

s(z) = (1 + z)^{- }/[(1 + z)^{- } - ½]

Figure 12 illustrates the cosmological function s(z) over redshift z, showcasing the best-fit model along with uncertainty bands for two parameters, β and . The central curve represents the most probable behavior of s(z) from z = -1 to z = 2, showing a smooth upward trend. Surrounding this curve, the blue shading captures the variation due to uncertainty in β (with an uncertainty of $±$0.013), while the purple shading reflects the range due to uncertainty in (with $±$0.0065). The best-fit values, $\beta = 1.312$ and = 1.273, provide insight into the expansion of the universe, helping refine our understanding of the cosmological model through these parameters and their uncertainties. The shape of the curve follows an upward trend as z transitions from negative values (future) through z = 0 (present) and into positive values (past). This behavior aligns with ΛCDM expectations.

The r–s plot in Figure 13 illustrates how different cosmological models behave, including uncertainty bands for the parameters $\beta = 1.312$ and = 1.273. These bands show how predictions shift within these uncertainty ranges. The ΛCDM model, often used as a baseline, is marked at (r, s) = (1, 0). Alternative models, like Chaplygin Gas and Quintessence, occupy other regions: Chaplygin Gas appears at higher r values with negative s, while Quintessence lies closer to ΛCDM but diverges with s < 0. These variations suggest different expansion paths for the universe, shedding light on how dark energy behaves according to each model.

Our model's trajectory starts at a certain point in the early universe (high z) and moves toward the ΛCDM point (1, 0) as the universe evolves. This convergence indicates that, despite differences in the theoretical formulation, our f(T) model ultimately behaves in a manner very similar to standard dark energy at late times.

The r–q plot in Figure 14 gives an overview of different cosmological models and how they predict the universe's expansion. The main blue line shows the

best-fit relationship between r and q based on the Hubble data, while shaded bands indicate uncertainty due to variations in two key parameters: $\beta = 1.312$ and = 1.273. These bands, in light blue for β and light coral for , show how much the model's predictions can shift due to small changes in these values.

Key points and regions on the plot help contextualize these models. The black dot at (-1, 1) represents the de Sitter (dS) point, where dark energy dominates, causing exponential expansion. The ΛCDM model—a standard reference in cosmology—is marked by an arrow pointing to the red dashed line at r = 1, showing where this model lies in the r–q space.

In addition, regions for alternative models are labeled: Chaplygin Gas appears in the upper left, associated with a specific dark energy model, while Quintessence lies closer to ΛCDM, suggesting a dynamic form of dark energy with slightly lower r values.

The plot also marks important transitions with vertical lines. The dashed line at q = -1 represents the boundary for the de Sitter expansion, while the solid line at q = 0 shows the shift from deceleration to acceleration in the expansion of the universe.

We also compare our model's behavior to other dark energy models. Quintessence models typically cluster close to, but slightly off, the ΛCDM line, while Chaplygin gas models occupy a different region of the plane. Our trajectory remains within the expected bounds of standard dark energy behavior, reinforcing that our f(T) model does not introduce exotic departures but rather mimics ΛCDM remarkably well.

3.6. Om Diagnostic

The Om diagnostic is a valuable tool for distinguishing between different dark energy models by comparing the universe's expansion rates. The expression for the Ω(z) parameter as a function of redshift z is given by:

$\Omega(z) = [H(z)/H_0]^2$ - $1/[(1 + z)^3$ - 1]

Using the specific form of H(z), we derive:

Ω(z) = [(1 + z)^{1+ }]^2 - $1/[(1 + z)^3$ - 1]

where β, , and H_0 are constants, and z represents the redshift.

Figure 15 illustrates the evolution of Ω(z), which is shown to be nearly flat as a function of z at low redshifts, taking a value around 0.3 (marked by a horizontal brown dashed line for reference Ω_{m0} = 0.3). We emphasize that in our model, Ω(z) approaches approximately 0.3 at z → 1, which is in excellent agreement with observations. We note that the curve is almost horizontal, indicating minimal deviation from ΛCDM expectations. These results provide strong evidence that our best-fit f(T) model closely mirrors the behavior of the standard ΛCDM cosmology. Despite its modified gravity foundation, the model

successfully replicates the expected cosmic evolution, reinforcing its viability as a realistic description of the expansion of the universe. The shaded regions, derived from uncertainties in the parameters $\beta = 1.312$ and $= 1.273$, highlight the robustness of the model over time. Notably, the influence of β becomes more prominent in the later stages of cosmic evolution. This strong alignment underscores the reliability of the model in describing the impact of dark energy on the expansion of the universe.

4. Discussion and Conclusion

In this research, we applied the energy-momentum tensor for a perfect fluid to solve the field equations within the f(T) gravity framework. From this approach, we derived essential cosmological parameters, including the Hubble parameter H and the deceleration parameter q, along with Om and Statefinder diagnostics, which help analyze the model's behavior relative to standard cosmological models. To enhance accuracy, we constrained the model parameters using the R^2-test, obtaining the best-fit values that closely match observational data.

Specifically, the best-fit curve for H(z) was generated from 57 observed data points, yielding an R^2 of 0.9527 and an RMSE of 9.2501. The strong alignment of our model with the established ΛCDM model highlights its reliability and accuracy in capturing the universe's expansion dynamics across the redshift range analyzed.

We calculated the AIC and BIC values to assess our model's performance. For our model, we obtained AIC_{Model} = 37.49 and BIC_{Model} = 43.82, based on a minimum chi-squared value ^2_{min} = 31.49. Compared to the ΛCDM model, which has AIC_ΛCDM = 40 and BIC_ΛCDM = 45, this gives ΔAIC = 2.51 and ΔBIC = 1.18. In line with findings from Jaybhaye et al. (2024), these results show moderate support for our model according to the AIC and strong support according to the BIC. This suggests that our model provides a solid fit to the data while effectively balancing simplicity and accuracy, making it a competitive alternative to the standard ΛCDM model.

We calculated the deceleration parameter q(z) and observed how it changes with redshift z, offering insights into the universe's expansion history. The graph highlights a key transition point where q(z) crosses zero (marked by the red dashed line), signaling the shift from a decelerating to an accelerating universe. The main curve represents the central values of q(z), while shaded areas show the range of possible values due to uncertainties in the parameters β and . Spanning redshifts from approximately -1.0 to 3.5, the figure captures the universe's journey from past deceleration to its present phase of accelerated expansion.

We further analyzed the behavior of pressure p, energy density , and the EoS parameter ω, plotting these variables over cosmic time t and redshift z using parameter values $\beta = 1.312$ and $= 1.273$. This study included two models: Model I, where $f(T) = \lambda T$, and Model II, where $f(T) = T + \beta T^2$. Both models align well with current observational data, including the Hubble and deceleration

parameters, suggesting they are effective in describing the universe's accelerated expansion. The energy condition graphs for Models I and II highlight both common trends and distinct features, offering unique insights into cosmological behavior.

In our analysis of the r–s and r–q diagnostics, we found that the pair (r, s) = (1, 0) and (r, q) = (1, -½) corresponds to the standard ΛCDM model. With best-fit parameters $\beta = 1.312$ and = 1.273, our model aligns closely with ΛCDM, confirming consistency with recent studies.

From the evolution of Ω(z), we observed a strong consistency with the ΛCDM model, as the Om parameter approaches the reference value of 0.3 at lower redshifts. The best-fit model closely aligns with ΛCDM, and the parameter uncertainties emphasize the model's reliability, with β's influence becoming more pronounced at higher redshifts.

Acknowledgments

P.S.G. acknowledges and expresses gratitude for fellowship provided by SARTHI. He sincerely appreciates SARTHI's commitment to supporting scholars and researchers and the positive impact the fellowship has had on his career. He also thanks DST-FIST for infrastructure support.

References

Arora, S., Pacif, S., Bhattacharjee, S., & Sahoo, P. 2020, *Physics of the Dark Universe*, 30, 100664
Bengochea, G. R., & Ferraro, R. 2009, *Physical Review D*, 79, 124019
Cai, Y.-F., Capozziello, S., De Laurentis, M., & Saridakis, E. 2016, *Reports on Progress in Physics*, 79, 106901
Capozziello, S., Gonzalez, P., Saridakis, E. N., & Vasquez, Y. 2013, *Journal of High Energy Physics*, 2013, 39
Chen, S.-H., Dent, J. B., Dutta, S., & Saridakis, E. N. 2011, *Physical Review D*, 83, 023508
Chen, R., Wang, Y.-Y., Zu, L., & Fan, Y.-Z. 2024, *Physical Review D*, 109, 024041
Dimakis, N., Christodoulakis, T., & Terzis, P. A. 2014, *Journal of Geometry and Physics*, 77, 97
Duchaniya, L., Lohakare, S. V., Mishra, B., & Tripathy, S. 2022, *European Physical Journal C*, 82, 448
Duran, I., Atrio-Barandela, F., & Pavón, D. 2012, *Journal of Cosmology and Astroparticle Physics*, 2012, 008
Farooq, O., Mania, D., & Ratra, B. 2013, *Astrophysical Journal*, 764, 138
Ferraro, R., & Fiorini, F. 2007, *Physical Review D*, 75, 084031
Geng, C.-Q., Lee, C.-C., & Saridakis, E. N. 2012, *Journal of Cosmology and Astroparticle Physics*, 2012, 002
Harko, T., Lobo, F. S., Nojiri, S., & Odintsov, S. D. 2011, *Physical Review D*,

84, 024020
Harko, T., Lobo, F. S., Otalora, G., & Saridakis, E. N. 2014, *Physical Review D*, 89, 124036
Izumi, K., & Ong, Y. C. 2013, *Journal of Cosmology and Astroparticle Physics*, 2013, 029
Jaybhaye, L. V., Solanki, R., & Sahoo, P. 2024, *Physics of the Dark Universe*, 46, 101639
Junior, E. L., Rodrigues, M. E., & Houndjo, M. J. 2015, *Journal of Cosmology and Astroparticle Physics*, 2015, 037
Karami, K., & Abdolmaleki, A. 2012, *Journal of Cosmology and Astroparticle Physics*, 2012, 007
Kolhatkar, A., Mishra, S. S., & Sahoo, P. 2024, *European Physical Journal C*, 84, 888
Krššák, M., Van Den Hoogen, R., Pereira, J., Böhmer, C., & Coley, A. 2019, *Classical and Quantum Gravity*, 36, 183001
Kumar, A., Sood, A., Singh, J., Beesham, A., & Ghosh, S. G. 2023, *Physics of the Dark Universe*, 40, 101100
Linder, E. V. 2010, *Physical Review D*, 81, 127301
Malik, A., Almas, A., Naz, T., & Manzoor, R. 2024, *European Physical Journal Plus*, 139, 587
Mandal, S., & Sahoo, P. 2021, *Physics Letters B*, 823, 136786
Mishra, B., Sahoo, P., & Varma, C. B. S. 2015, *International Journal of Pure and Applied Mathematics*, 99, 109
Mohanty, G., & Mishra, B. 2001, *Czech Journal of Physics*, 51, 525
Mohanty, G., & Mishra, B. 2003, *Astrophysics and Space Science*, 283, 67
Naicker, S., Maharaj, S. D., & Brassel, B. P. 2023, *Universe*, 9, 47
Narawade, S. A., & Mishra, B. 2023, *Annalen der Physik*, 535, 2200626
Nunes, R. C., Barboza, E. M., Abreu, E. M., & Neto, J. A. 2016, *Journal of Cosmology and Astroparticle Physics*, 2016, 051
Pawar, D., & Mapari, R. 2022, *Journal of Dynamical Systems and Geometric Theories*, 20, 115
Pawar, D., Mapari, R., & Pawade, J. 2021, *Pramana*, 95, 10
Pawar, D., Raut, D., & Patil, W. 2023, *New Astronomy*, 100, 101999
Pawar, D., Ghungarwar, N., & Gaikwad, P. 2024b, *East European Journal of Physics*, 1, 102
Pawar, D., Raut, D., & Kale, A. 2024c, *New Astronomy*, 110, 102214
Pawar, D., Gaikwad, P., Muhammad, S., & Zotos, E. E. 2024a, *Astronomy and Computing*, 48, 100847
Pawar, D., Raut, D., Nirwal, A., Singh, J., et al. 2024d, *Astronomy and Computing*, 48, 100848
Pawar, D., Gaikwad, P., Muhammad, S., & Zotos, E. E. 2025a, *Physics of the Dark Universe*, 47, 101100
Pawar, D., Ghungarwar, N., Muhammad, S., & Zotos, E. 2025b, *Astronomy and Computing*, 51, 100900
Pradhan, A., & Mathur, P. 2009, arXiv:0806.4815
Pradhan, A., & Ram, P. 2009, *International Journal of Theoretical Physics*, 48,

3188
Pradhan, A., Dixit, A., et al. 2020, arXiv:2009.08290
Pradhan, A., Goswami, G., Rani, R., & Beesham, A. 2023, *Astronomy and Computing*, 44, 100700
Rani, S., Singh, J., & Sharma, N. 2015, *International Journal of Theoretical Physics*, 54, 1698
Rao, V., Sireesha, K., & Papa Rao, D. C. 2014, *European Physical Journal Plus*, 129, 1
Sahoo, P., Taori, B., & Mahanta, K. 2020, *Canadian Journal of Physics*, 98, 1015
Setare, M., & Darabi, F. 2012, *General Relativity and Gravitation*, 44, 2521
Shaikh, A. 2016, *International Journal of Theoretical Physics*, 55, 3120
Shekh, S., Bouali, A., Mustafa, G., Pradhan, A., & Javed, F. 2023, *Classical and Quantum Gravity*, 40, 135006
Shukla, B. K., Sofuoğlu, D., Khare, S., & Alfedeel, A. H. 2025, *International Journal of Geometric Methods in Modern Physics*, 22, 2450015
Singh, C., & Singh, V. 2014, *General Relativity and Gravitation*, 46, 1696
Singh, J., Shaily, Ram, S., Santos, J. R., & Fortunato, J. A. 2023, *International Journal of Modern Physics D*, 32, 2350015
Sofuoğlu, D., Baysal, H., & Tiwari, R. 2023, *European Physical Journal Plus*, 138, 1
Solanke, Y., Kale, A., Pawar, D., & Dagwal, V. 2023, *Canadian Journal of Physics*, 102, 85
Sood, A., Ali, M. S., Singh, J., & Ghosh, S. G. 2024, *Chinese Physics C*, 48, 065109
Tamanini, N., & Boehmer, C. G. 2012, *Physical Review D*, 86, 044009
Tiwari, R., Sofuoğlu, D., & Dubey, V. 2020, *International Journal of Geometric Methods in Modern Physics*, 17, 2050187
Tiwari, R. K., Shukla, B. K., Sofuoğlu, D., & Kösem, D. 2023, *Symmetry*, 15, 788
Wang, D., & Mota, D. 2020, *Physical Review D*, 102, 063530
Yadav, A. K., Bhoyar, S., Dhabe, M., Shekh, S., & Ahmad, N. 2024, *Journal of High Energy Astrophysics*, 43, 114

Figures

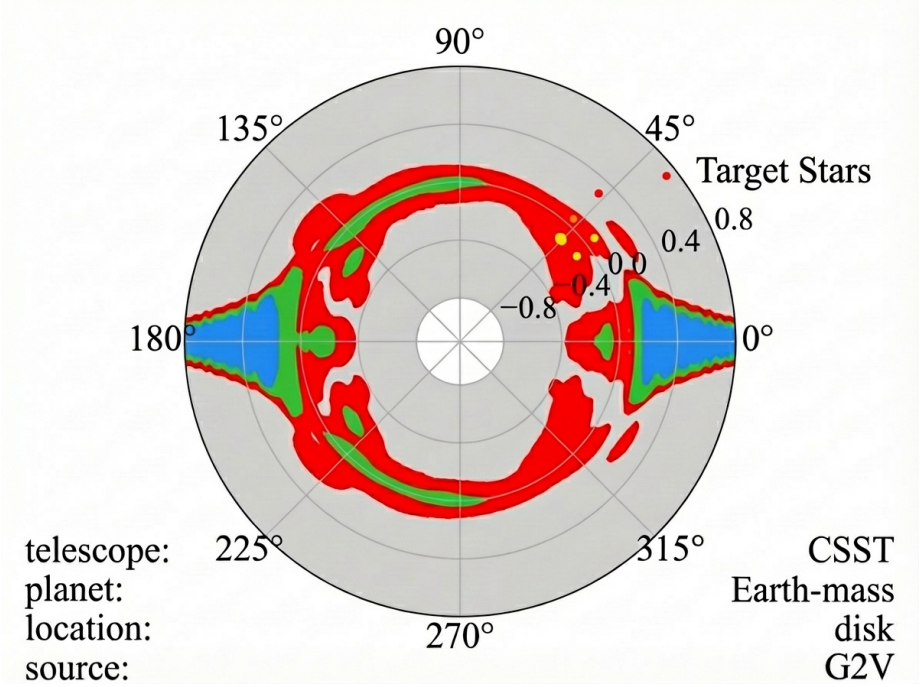

Figure 1: Figure 10